Solar Energy Materials and Solar Cells 178 (2018) 266–272

Contents lists available at ScienceDirect

Solar Energy Materials and Solar Cells

journal homepage: www.elsevier.com/locate/solmat

Comprehensive photonic approach for diurnal photovoltaic and nocturnal radiative cooling

Bin Zhao, Mingke Hu, Xianze Ao, Qingdong Xuan, Gang Pei*

Department of Thermal Science and Energy Engineering, University of Science and Technology of China, Hefei 230027, China

ARTICLE INFO

Keywords:
Photonics
Photovoltaic
Radiative cooling
Solar cells

ABSTRACT

A novel photovoltaic/radiative cooling (PV/RC) hybrid system based on a selective plate is proposed. This system can generate electricity via diurnal PV conversion and obtain cooling energy by radiative cooling. We introduce a comprehensive photonic approach to simultaneously reduce impractical solar radiation absorption of the selective plate and enhance its thermal radiation for the hybrid system. Initially, we design a photonic structure made of 1D multilayer stack and 2D photonic crystal, which can selectively reflect solar radiation and actively radiate heat to the outer space while maintaining its solar transmission in PV conversion band (0.3–1.1 μm). Then, we demonstrate that applying the photonic structure to a monocrystalline silicon solar cell can obtain a diurnal electricity output of 99.2 W m^{-2} and generate a nocturnal RC power by 128.5 W m^{-2}, indicating 6.9% and 30.5% higher than those of a bare cell. In addition, the potential cooling energy obtained is far more in this structure than in existing RC emitters, including daytime RC emitter reported in a recent research. Results indicate that a comprehensive photonic approach can be used to design spectral selective structures for advancing the applications of exploiting solar energy harvesting and radiative cooling utilization.

1. Introduction

The universe, at a temperature of 3 K, represents a significant renewable thermodynamic resource; it is the ultimate heat sink [1]. The atmosphere of the earth exhibits remarkably high transmittance for electromagnetic waves within the atmospheric window band (8–13 μm) that coincides with the peak wavelength of thermal radiation of a blackbody at a typical ambient temperature. Thus, terrestrial objects with high emissivity within the atmospheric window band can obtain cooling energy by radiating heat to outer space when these objects are directly exposed to the sky. This passive radiative cooling mechanism has recently drawn a considerable attention for its potential as an alternative method for thermal management.

Radiative cooling is largely investigated simply because of a single radiative cooling system (RC system) at nighttime to obtain cooling energy in previous studies [2–11]. Spectral selective-independent and spectral selective-dependent emitters are successively developed for utilizing a nocturnal RC process. Daytime RC has been achieved in recent years [12–17]. Specifically, a photonic structure that consists of seven alternating layers of hafnium dioxide (HfO_2) and silicon dioxide (SiO_2) on top of a silver layer and a silicon wafer is reported to cool below the ambient temperature at approximately 5 °C via RC method [13]. This photonic structure can reflect approximately 97% of incident solar irradiance and simultaneously emit remarkably thermal radiation. However, a comparatively low cooling power and high investment are the main challenges for a single RC system in practical applications. By contrast, existing solar energy harvesting systems, including photovoltaic (PV) system (silicon-based cells [18], perovskite-based cells [19] and et al.) and photothermal (PT) system, are also single units working only at daytime. For these applications, the RC method can possibly combine with these systems to simultaneously obtain nocturnal cooling energy and preserve the function of harvesting diurnal solar energy.

In this work, we propose a PV/RC hybrid system based on a selective plate; this system can generate electricity by diurnal PV conversion and obtain cooling energy via nocturnal RC process (Fig. 1). Only solar irradiation with a certain wavelength range (0.3–1.1 μm for monocrystalline silicon solar cell) can be partly converted into electricity for PV conversion technique, and the remaining absorbed solar irradiation is dissipated into heat. However, a 1 K increase in temperature decreases the relative efficiency of the crystalline silicon solar cells by approximately 0.45%. Thus, the selective plate of the PV/RC hybrid system must have a high solar absorption within the PV conversion band to ensure a diurnal PV electricity output and actively reflect the remaining solar irradiation to prevent solar cell from overheating. Moreover, the selective plate should also be powerfully emissive within the mid-infrared band (4–25 μm), thereby allowing the system to

* Corresponding author.
E-mail address: peigang@ustc.edu.cn (G. Pei).

https://doi.org/10.1016/j.solmat.2018.01.023
Received 6 October 2017; Received in revised form 17 December 2017; Accepted 15 January 2018
Available online 06 February 2018
0927-0248/

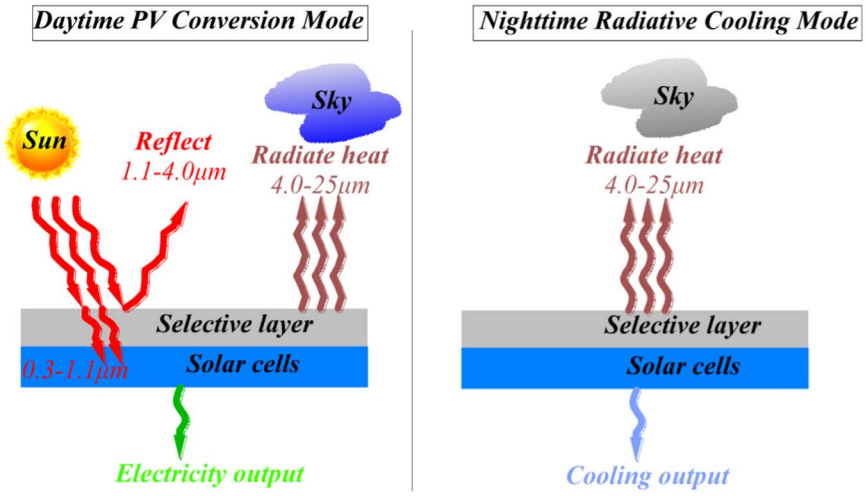

Fig. 1. Schematic of diurnal PV conversion and nocturnal RC process of the selective plate.

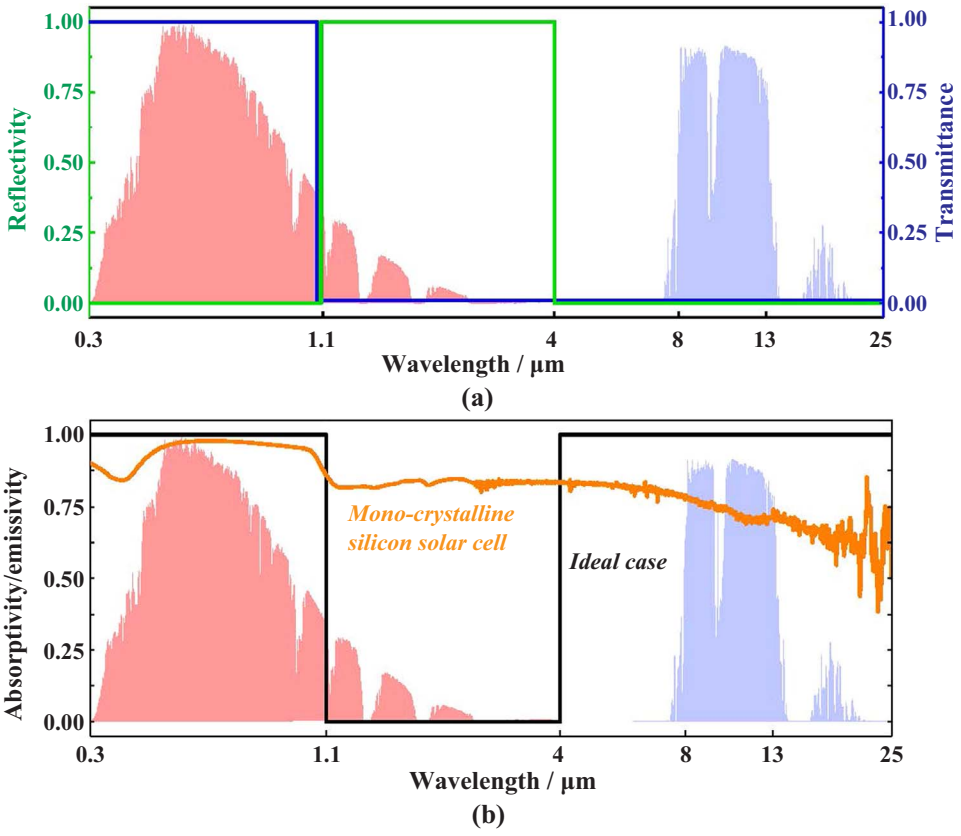

Fig. 2. Idealized spectral selectivity of the selective plate from the ultraviolet to mid-infrared, with the normalized AM 1.5 solar spectrum (red) and typical atmospheric transmittance (blue) plotted for reference. The ideal selective plate demonstrates a high spectral absorptivity (emissivity) in the wavelength range of 0.3–1.1 μm and beyond 4.0 μm, with high reflectivity in the wavelength range of 1.1–4.0 μm. (a) Ideal reflectivity (green curve) and transmittance (blue curve) of the selective layer placed at the top of solar cells. (b) Ideal absorptivity (emissivity) of the selective plate (black curve) comprehensively considering the influence of selective layer and solar cell. The absorptivity (emissivity) of monocrystalline silicon solar cell (orange curve), which was measured by UV–Vis–NIR spectrophotometer (DUV-3700) and Fourier transform infrared spectrophotometer (Nicolet iS10), is plotted for reference. (For interpretation of the references to color in this figure legend, the reader is referred to the web version of this article.).

produce considerable nocturnal RC power. The high emissivity of a selective plate is better with the mid-infrared band (4–25 μm) than simply within atmospheric window band (8–13 μm) for cooling solar cells in the diurnal PV process [15]. Fig. 2 illustrates an idealized spectral-selective profile of the selective plate, with the spectral absorptivity (emissivity) of the monocrystalline silicon solar cell plotted for reference.

In this work, we develop a comprehensive photonic approach for designing a selective plate for the PV/RC system. This approach aims to place a photonic structure on top of a monocrystalline silicon solar cell. The photonic structure should satisfy multiple spectral characteristics. First, the photonic structure should maximize transmittance in the wavelength range of 0.3–1.1 μm (or *PV band*) to ensure the PV conversion of monocrystalline silicon solar cell. Second, the photonic structure must have high reflectivity in the wavelength range of 1.1–4.0 μm (or *vain band*) to reflect part of solar irradiance that cannot be converted to electricity, thus reducing the temperature of the solar cell. Third, the emissivity of the photonic structure in the wavelength range of 4.0–25 μm (or *RC band*) is designed to be high to maximize the RC process. The diurnal PV conversion and nocturnal RC process, which is a new concept of energy harvesting by exploiting solar energy and radiative cooling applications, can be successfully achieved by placing this photonic structure on a monocrystalline silicon solar cell.

2. Materials and methods

2.1. Design principle and results

In this section, we introduce our design principle for a photonic structure that is placed on a monocrystalline silicon solar cell to satisfy

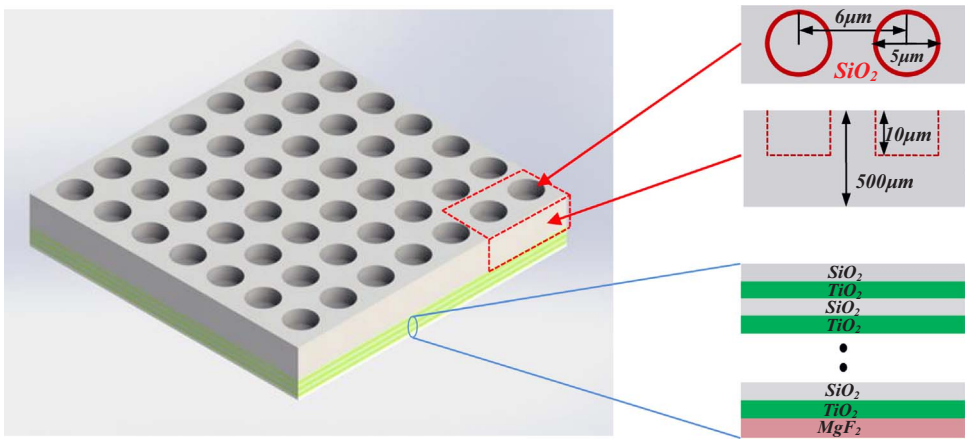

Fig. 3. Schematic of a photonic structure. The photonic structure consists of a 1D multilayer stack and a 2D photonic crystal. The 1D multilayer stack is composed of 30 SiO_2/TiO_2 layers periodically and a single MgF_2 layer at the bottom. The 2D photonic crystal is a 500 μm-thick silica with a specific circular lattice array on the top surface. The circular lattice array has the following parameters: diameter = 5 μm, period = 6 μm, and depth = 10 μm.

the spectral characteristics of the selective plate. We develop a comprehensive photonic approach for photonic structure by integrating a 1D multilayer stack and a 2D photonic crystal. In Fig. 3, the alternative silicon dioxide (SiO_2) and titanium dioxide (TiO_2) layers are at the back of a 2D photonic crystal, with a single MgF_2 at the bottom. The 2D photonic crystal, which we will refer to as "photonic substrate," is a 500 μm-thick silica with a circular lattice of 5 μm diameter, 10 μm depth, and 6 μm periodicity on the top surface. The 1D multilayer stack assists in optimizing the reflectivity of the photonic structure in the *vain band*. The photonic substrate is responsible for enhancing the thermal radiation of the selective plate. We select TiO_2 and SiO_2 as the basic materials for our 1D multilayer stack [20–23]. TiO_2 serves as a high-index material with low absorptivity in the solar radiation band, which is a useful feature when optimizing the reflectivity of the photonic structure in the *vain band*. SiO_2 is a low-index material and is optically transparent to solar radiation. Meanwhile, SiO_2 has a high extinction coefficient over thermal radiation band at typical temperature, which is fit for thermal radiation enhancement naturally. However, SiO_2 has a negative permittivity near 9 μm because of its strong phonon–polariton resonance, leading to a large reflectivity but minimal emissivity. However, this emissivity drop coincides with the atmospheric window that is the peak blackbody radiation wavelength for objects at terrestrial temperature. Thus, we design a circular lattice array on top of a 500 μm silica to overcome this deficiency.

The optimization of the multilayer stack is performed through the needle method [24], and the spectral characteristics of the entire photonic structure are calculated over an ultrabroadband wavelength between 0.3 and 25 μm with a wavelength step size of 0.002 μm through the rigorous coupled-wave analysis method [25]. Fig. 4 presents the spectral characteristics of the optimized photonic structure. The photonic structure has high reflectivity in the *vain band*, and the weighted reflectivity of the photonic structure in the *vain band* is 63.0%, reflecting solar irradiance of 123 W m^{-2} with reference to the standard AM 1.5 solar irradiance. In the *PV band*, the photonic structure is optically transparent, and the weighted transmittance is 91.0%, which is consistent with the transmittance of 3.2 mm glass used in the conventional PV panel. In addition, this photonic structure shows that a broadband high emissivity is better in the *RC band* than in the aforementioned 3.2 mm glass. Therefore, adding this photonic structure on top of a monocrystalline silicon solar cell for the selective plate is beneficial for PV conversion and RC processes.

2.2. Thermal simulation

We use the following 1D thermal model to evaluate the diurnal electricity output and nocturnal RC power of the selective plate and analyze the realistic performance of the selective plate. Fig. 5 illustrates the schematic of this model. The aluminum plate in Fig. 5 acts as a substrate for solar cell in the actual manufacturing process.

We disregard the temperature variation of the selective plate in the horizontal direction and assume that the solar cells contribute the total solar radiation absorbed by the selective plate. The steady-state heat diffusion equation of the selective plate based on the aforementioned assumptions is expressed as follows [26,27]:

$$\frac{d}{dH}\left(k\frac{dT}{dH}\right) + \dot{q} = 0, \tag{1}$$

where T is the temperature distribution of the selective plate in H direction, K. k is the thermal conductivity of the selective plate along the H direction, W m^{-1} K^{-1}. In particular, the thermal conductivities of silicon solar cell, silica, and aluminum are at 148, 1.38, and 237 W m^{-1} K^{-1}, respectively [26,28]. $\dot{q}$ is the internal heating source generated by parts of the absorbed solar radiation that cannot be converted to electricity and dissipated to heat. $\dot{q}$ is expressed as follows:

$$\dot{q} = P_{sun} - E_{pv}, \tag{2}$$

where P_{sun} is the solar radiation absorbed by the selective plate, W m^{-2}. E_{pv} is the electricity output generated by the solar cell, W m^{-2}.

The boundary conditions of this structure are defined as follows:

$$\text{Top surface:} \quad -k\frac{dT}{dH}\Big|_{H=H_{max}} = P_{rad}(T_{top}) - P_{sky}(T_{amb}) + P_{non-rad}(T_{top}, T_{amb}), \tag{3}$$

$$\text{Bottom surface:} \quad k\frac{dT}{dH}\Big|_{H=0} = P_{non-rad}(T_{bottom}, T_{amb}), \tag{4}$$

In Eq. (2), P_{sun} is the absorbed solar radiation by the selective plate, which is expressed as follows:

$$P_{sun} = G\cdot\alpha_p, \tag{5}$$

where G is the total solar radiation, W m^{-2}. α_p is the absorptivity of the selective plate weighted by the standard AM 1.5 solar spectrum for solar radiation.

In Eq. (2), E_{pv} is the electricity output generated by solar cells. E_{pv} in existing solar energy harvesting systems [29–31], including the PV system, considering the influence of the temperature of a solar cell can be expressed as follows [30]:

$$E_{pv} = G\alpha_p\eta_{ref}[1 - Br(T_{pv} - T_{ref})], \tag{6}$$

where η_{ref} is the reference efficiency of the solar cell measured at a standard condition (T = 298.15 K, G = 1000 W m^{-2}); T_{ref} is the reference temperature, T_{ref} = 298.15 K; B_r is the temperature coefficient of PV efficiency for a solar cell, K^{-1}; and T_{pv} is the temperature of the solar cell. We modify the expression of E_{pv} for the selective plate based on Eq. (6):

$$E_{pv} = G_{0.3-1.1}\alpha_{0.3-1.1}\eta_{ref}[1 - Br(T_{pv} - T_{ref})]/\varphi, \tag{7}$$

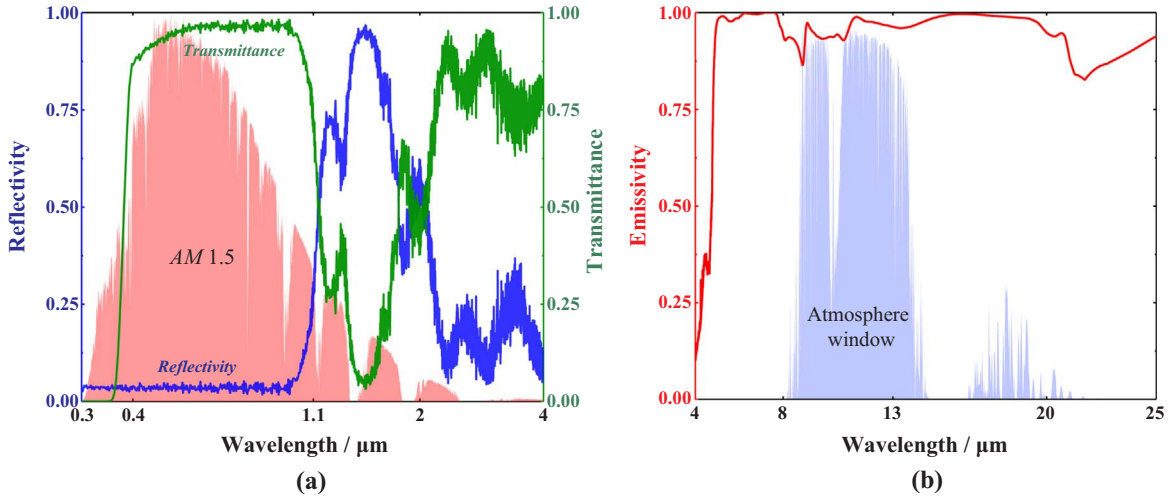

Fig. 4. Spectral selectivity of the photonic structure, with the normalized AM 1.5 solar spectrum (red) and typical atmospheric transmittance (blue) plotted for reference. (a) Spectral reflectivity (blue curve) and transmittance (green curve) of the photonic structure in the solar radiation band. (b) The spectral emissivity (red curve) of the photonic structure in the mid-infrared wavelength band. (For interpretation of the references to color in this figure legend, the reader is referred to the web version of this article.).

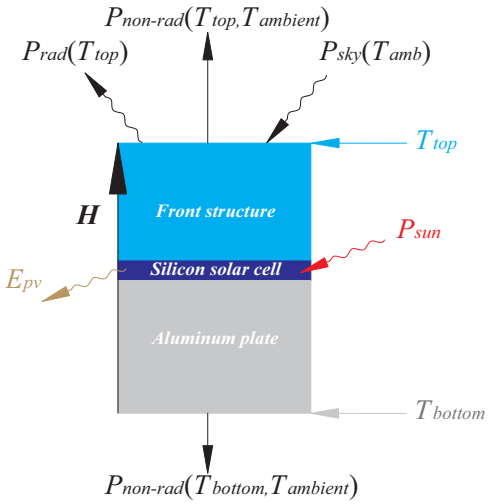

Fig. 5. Schematic of the 1D thermal mathematical model. T_{top} and T_{bottom} refer to the temperature of the top and bottom surfaces, respectively. T_{amb} represents ambient temperature, and $P_{non\text{-}rad}$ is the comprehensive effects of convection and conduction.

where $G_{0.3\text{–}1.1}$ is the solar radiation energy in the *PV band* that coincides with the spectral response of silicon solar cell, W m^{-2}; and φ is the proportion of $G_{0.3\text{–}1.1}$ in the whole solar radiation energy G, $\varphi = G_{0.3\text{–}1.1}/G$; $\alpha_{0.3\text{–}1.1}$ is the weighted absorptivity of the selective plate within *PV band*.

In Eq. (3), P_{rad} (T_{top}) is the power density radiated out by the top surface:

$$P_{rad}(T_{top}) = \int_0^{\infty}\int_0^{2\pi}\int_0^{\pi/2} I_{\lambda,b}(\lambda, T_{top})\ \varepsilon_p(\lambda, \theta, \varphi)cos\theta sin\theta d\theta d\varphi d\lambda, \quad (8)$$

where ε_p (λ,θ,φ) and $I_{\lambda,b}$ (λ,T_{top}) denote the directional spectral emissivity of the structure and spectral radiance of a blackbody, respectively, at temperature T_{top}. $I_{\lambda,b}$ (λ,T_{top}) is expressed as follows:

$$I_{\lambda,b}(\lambda, T_{top}) = 2hc_0^2\lambda^{-5}/\{exp[hc_0/(\lambda k_b T_{top})] - 1\}, \quad (9)$$

where h is the Planck constant ($h = 6.626 \times 10^{-34}$ J s), k_b is the Boltzmann constant ($k_b = 1.381 \times 10^{-23}$ J K^{-1}), and c_0 is the velocity of light, m s^{-1}.

In Eq. (3), P_{sky} (T_{amb}) is the absorbed power density from the atmosphere:

$$P_{sky}(T_{amb}) = \int_0^{\infty}\int_0^{2\pi}\int_0^{\pi/2} I_{\lambda,b}(\lambda, T_{amb})\ \alpha_p(\lambda, \theta, \varphi)\varepsilon_{sky}(\lambda, \theta, \varphi)cos\theta sin\theta d\theta d\varphi d\lambda, \quad (10)$$

where $\alpha_p(\lambda,\theta,\varphi)$ is the directional spectral absorptivity of the selective plate. $\alpha_p(\lambda,\theta,\varphi)$ can be replaced by $\varepsilon_p(\lambda,\theta,\varphi)$ according to Kirchhoff's radiation law. $\varepsilon_{sky}(\lambda,\theta,\varphi)$ is the directional spectral emissivity of the atmosphere and can be derived from empirical correlations [32,33] or obtained by commercial software, such as MODTRAN [34].

In Eqs. (3) and (4), $P_{non\text{-}rad}(T, T_{amb})$ is the power density driven by conductive and convective heat transfer processes:

$$P_{non-rad}(T_{top}, T_{amb}) = h_{top}(T_{top} - T_{amb}), \quad (11)$$

$$P_{non-rad}(T_{bottom}, T_{amb}) = h_{bottom}(T_{bottom} - T_{amb}), \quad (12)$$

where h_{top} and h_{bottom} are the heat transfer coefficients of a non-radiative process at the top and back surfaces, respectively, W m^{-2} K^{-1}.

We use diurnal electricity output E_{pv} and nocturnal RC power $P_{net\_cooling}$ to evaluate the PV and RC performance of the selective plate, respectively. E_{pv} is confirmed by using Eq. (7), whereas $P_{net\_cooling}$ is determined as follows:

$$P_{net,cooling}(T_{top}) = P_{rad}(T_{top}) - P_{sky}(T_{amb}) - P_{sun} + E_{pv} + P_{non-rad}(T_{top}, T_{amb}), \quad (13)$$

where P_{sun} and E_{pv} are 0 at nighttime and have no effect on $P_{net\_cooling}$. Considering that the net RC power is obtained by the heat exchange between the aluminum plate and working fluid (e.g., air) in actual applications, $P_{net\_cooling}$ can be also determined as follows.

$$P_{net,cooling} = h_{bottom}(T_{fluid} - T_{bottom}) \quad (14)$$

We select an ideal and three real cases for our simulation to evaluate the performance of the selective plate for PV and RC (Table 1). The photonic case in Table 1 is the selective plate discussed above.

Table 1
Information of the different cases for simulation.

Name of case	Type of solar cell	Type of front structure
Photonic case (selective plate)	Silicon solar cell	Photonic structure
Glass/glass case	Silicon solar cell	3.2 mm glass
Bare/bare case	Silicon solar cell	None
Ideal/ideal case	Silicon solar cell	Ideal surface

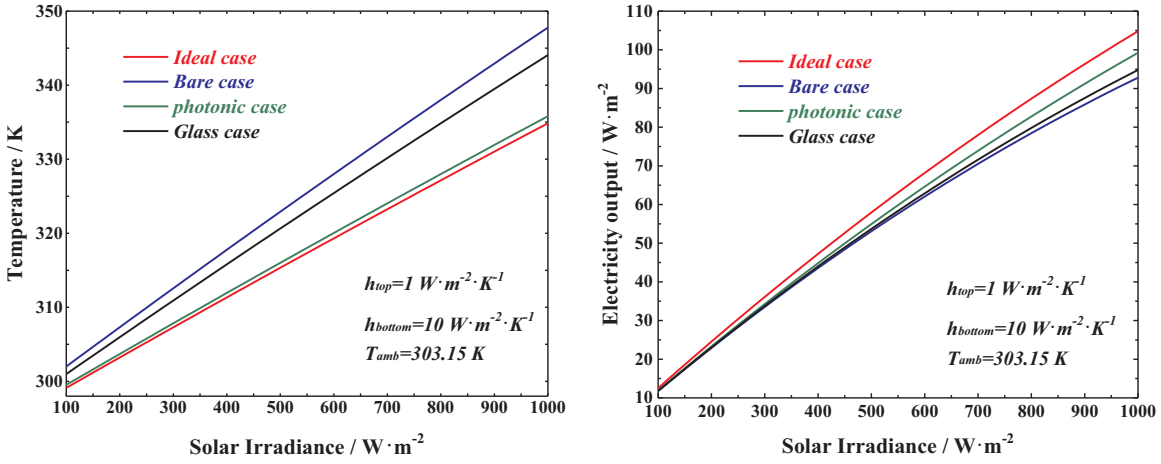

Fig. 6. (a) Operating temperature of solar cells in different cases. (b) Electricity output of the different cases. The ambient temperature T_{amb} is set to 303.15 K for both (a) and (b).

3. Results and discussions

3.1. Diurnal PV performance

The operating temperature of the solar cell and the electricity output of the selective plate with different solar irradiances are presented in Figs. 6(a) and 6(b). During the simulation, h_{top} and h_{bottom} are set as 1 and 10 W m^{-2} K^{-1}, correspondingly, which is near the realistic condition [35], with η_{ref} set as 12.5%. Fig. 6(a) shows that the operating temperature of a solar cell in the photonic case is the lowest among the three real cases, indicating that the designed photonic structure could significantly reduce the operating temperature of the solar cell during the diurnal PV conversion process. This result is mainly contributed by the robust reflectivity of the photonic structure in the *vain band*. For example, the operating temperature of the solar cell at 1000 W m^{-2} solar irradiation in the photonic case is 335.8 K, which is 12.0 K lower than that in the bare case and 8.3 K lower than that in the glass case. Such a temperature drop will significantly improve the PV efficiency of the selective plate, considering the negative temperature coefficient of approximately −0.45% on the PV efficiency for silicon solar cell. Fig. 6(b) demonstrates that the electricity output of the photonic case is the largest among the three real cases. The electricity output of the photonic case at 1000 W m^{-2} solar irradiation is 99.2 W m^{-2}, which is 6.9% higher than that of the bare case and 4.6% higher than that of the glass case, thereby proving that the photonic case has better diurnal PV performance than the bare and glass cases.

3.2. Nocturnal RC performance

Fig. 7 presents the nocturnal RC powers of the different cases. The photonic case has a larger nocturnal RC power than the bare and glass cases. Specifically, the photonic case achieves a nocturnal RC power of 128.5 W m^{-2} at 303.15 K, which is 30.5% higher than the bare case and 9.3% higher than the glass case, which demonstrates that the photonic case exhibits considerable performance for the nocturnal RC process. This scenario also implies that the nocturnal RC power could be enhanced by modifying the emissivity of structure in the *RC band*.

3.3. Effects of h_{bottom} on PV and RC performance

We investigate the effects of h_{bottom} on PV and RC performances of the photonic case. The large h_{bottom} equates to the favorable heat exchange process between the aluminum plate and working fluid (e.g., air). In Fig. 8, the electricity output and the RC power of photonic case increase gradually when h_{bottom} increases. This result implies that h_{bottom} will enhance the performance of the diurnal PV conversion and nocturnal RC processes.

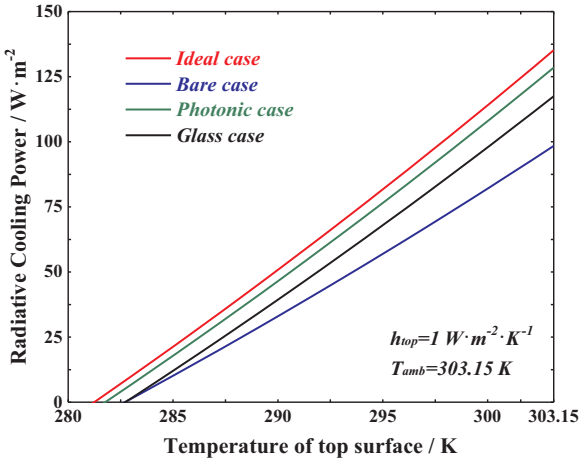

Fig. 7. Nocturnal RC power of different cases. h_{top} was set as 1 W m^{-2} K^{-1}. The ambient temperature T_{amb} was considered 303.15 K.

3.4. RC performance comparison with existing RC emitters

We select two kinds of single RC emitters for comparison under realistic climate condition in May at Hefei, China (32° N, 117°E). The two kinds of single RC emitters are the typical nocturnal RC emitter with high emissivity in the wavelength range of 8–13 μm [36] and the daytime RC emitter, which functions day and night, reported in a recent research [13]. The weather data of Hefei are provided by EnergyPlus software [37]. In this work, we use the equivalent cooling energy Q_{ec} obtained in the entire month to compare the RC performance. Q_{ec} is calculated by the following equation:

$$Q_{ec} = (P_{net\,cooling} + E_{pv} \times EER) \times \Delta t, \quad (15)$$

where *EER* is the energy efficiency ratio of the typical air conditioner, and Δt is time. *EER* is selected as 3.20 according to the Chinese National Standard [38].

Fig. 9 presents that the equivalent cooling energy obtained by the photonic case is far more than that of daytime RC emitter and nocturnal RC emitter. For example, the equivalent cooling energy of the photonic case is 238.8 MJ m^{-2}, which is 124.2% higher than that of daytime RC emitter. This result indicates that the photonic case has the enticing potential for cooling, which provides a possible means for exploiting an

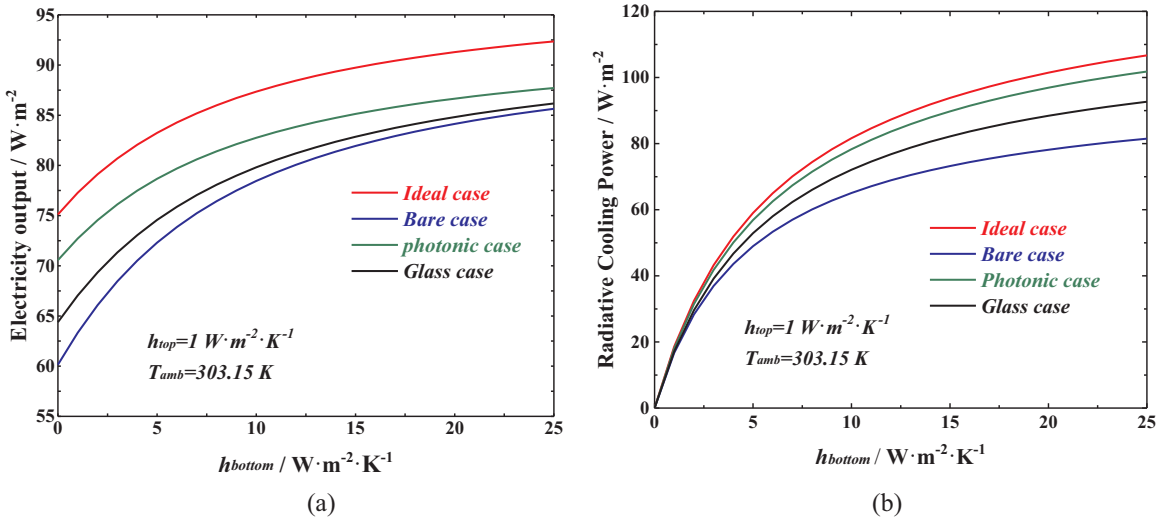

Fig. 8. (a) Diurnal electricity output of the different cases under different h_{bottom}. (b) Nocturnal RC power of the different cases under different h_{bottom}. h_{top} was set as 1 W m^{-2} K^{-1}. The ambient temperature T_{amb} was set to 303.15 K for both (a) and (b).

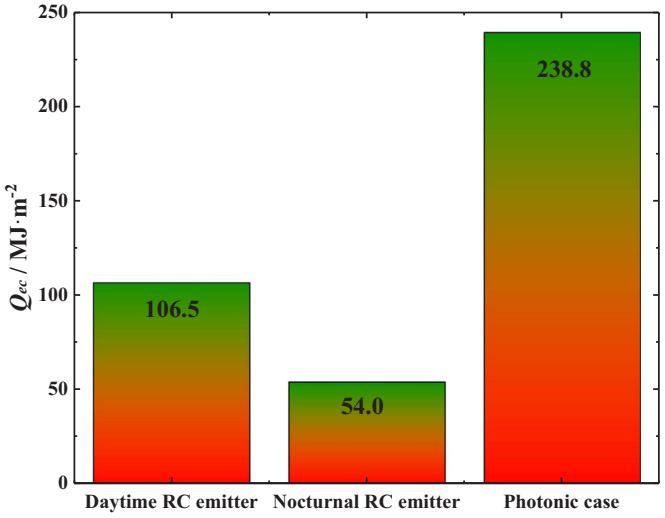

Fig. 9. Equivalent cooling energy of the daytime/nocturnal RC emitter and photonic case.

untapped degree of freedom for cooling energy harvesting.

4. Conclusions

In summary, we propose a PV/RC hybrid system for diurnal PV conversion and nocturnal RC processes to obtain electricity and cooling energy. Then, we introduce a comprehensive photonic approach for the selective plate by placing a photonic structure on top of a monocrystalline silicon solar cell. The photonic structure is designed to simultaneously enhance the RC process and reduce the useless solar absorption of the selective plate. We designed a photonic structure, which consists of a 1D multilayer stack and a 2D photonic crystal to satisfy the aforementioned demand. Then, a thermal simulation is conducted to investigate the performance of the designed photonic structure on the diurnal PV conversion and nocturnal RC processes. The results show that this photonic structure can not only effectively reduce the cell operating temperature in the diurnal PV conversion but also exhibit a large net RC power in the nocturnal RC process, thereby proving that this photonic structure has the enticing potential for the PV/RC hybrid system. In addition, the cooling energy obtained by the proposed selective plate is far more than that of existing RC emitters. This comprehensive photonic approach can also be applied to any other solar cells for different applications [35,39], although the presented photonic structure is designed for monocrystalline silicon solar cell in the PV/RC hybrid system. This work advances the applications of exploiting solar energy harvesting and radiative cooling utilization.

Acknowledgments

This work was supported by the National Natural Science Foundation of China (NSFC 51476159 and 51776193), Dongguan Innovative Research Team Program (No. 2014607101008), International Technology Cooperation Program of the Anhui Province of China (BJ2090130038), Fundamental Research Funds for the Central Universities, and National Postdoctoral Program for Innovative Talents (BX201700223).

References

[1] L. Zhu, A.P. Raman, S. Fan, Radiative cooling of solar absorbers using a visibly transparent photonic crystal thermal blackbody, Proc. Natl. Acad. Sci. USA 112 (2015) 12282–12287.
[2] C. Granqvist, A. Hjortsberg, Radiative cooling to low temperatures: general considerations and application to selectively emitting SiO films, J. Appl. Phys. 52 (1981) 4205–4220.
[3] P. Berdahl, Radiative cooling with MgO and/or LiF layers, Appl. Opt. 23 (1984) 370–372.
[4] B. Orel, M.K. Gunde, A. Krainer, Radiative cooling efficiency of white pigmented paints, Sol. Energy 50 (1993) 477–482.
[5] M. Al-Nimr, M. Tahat, M. Al-Rashdan, A night cold storage system enhanced by radiative cooling—a modified Australian cooling system, Appl. Therm. Eng. 19 (1999) 1013–1026.
[6] M. Meir, J. Rekstad, O. LØvvik, A study of a polymer-based radiative cooling system, Sol. Energy 73 (2002) 403–417.
[7] D. Beysens, M. Muselli, I. Milimouk, C. Ohayon, S.M. Berkowicz, E. Soyeux, M. Mileta, P. Ortega, Application of passive radiative cooling for dew condensation, Energy 31 (2006) 2303–2315.
[8] H. Bagiorgas, G. Mihalakakou, Experimental and theoretical investigation of a nocturnal radiator for space cooling, Renew. Energy 33 (2008) 1220–1227.
[9] A.R. Gentle, G.B. Smith, Radiative heat pumping from the earth using surface phonon resonant nanoparticles, Nano Lett. 10 (2010) 373–379.
[10] G. Smith, Amplified radiative cooling via optimised combinations of aperture geometry and spectral emittance profiles of surfaces and the atmosphere, Sol. Energy Mater. Sol. Cells 93 (2009) 1696–1701.
[11] A.R. Gentle, K.L. Dybdal, G.B. Smith, Polymeric mesh for durable infra-red transparent convection shields: applications in cool roofs and sky cooling, Sol. Energy Mater. Sol. Cells 115 (2013) 79–85.
[12] E. Rephaeli, A. Raman, S. Fan, Ultrabroadband photonic structures to achieve high-performance daytime radiative cooling, Nano Lett. 13 (2013) 1457–1461.
[13] A.P. Raman, M.A. Anoma, L. Zhu, E. Rephaeli, S. Fan, Passive radiative cooling below ambient air temperature under direct sunlight, Nature 515 (2014) 540–544.
[14] Z. Chen, L. Zhu, A. Raman, S. Fan, Radiative cooling to deep sub-freezing temperatures through a 24-h day–night cycle, Nat. Commun. 7 (2016) 13729.

[15] J.-l. Kou, Z. Jurado, Z. Chen, S. Fan, A.J. Minnich, Daytime radiative cooling using near-black infrared emitters, ACS Photonics 4 (2017) 626–630.
[16] Y. Zhai, Y. Ma, S.N. David, D. Zhao, R. Lou, G. Tan, R. Yang, X. Yin, Scalable-manufactured randomized glass-polymer hybrid metamaterial for daytime radiative cooling, Science 355 (2017) 1062–1066.
[17] Z. Huang, X. Ruan, Nanoparticle embedded double-layer coating for daytime radiative cooling, Int. J. Heat Mass Transf. 104 (2017) 890–896.
[18] J. Eisenlohr, N. Tucher, H. Hauser, M. Graf, J. Benick, B. Bläsi, J.C. Goldschmidt, M. Hermle, Efficiency increase of crystalline silicon solar cells with nanoimprinted rear side gratings for enhanced light trapping, Sol. Energy Mater. Sol. Cells 155 (2016) 288–293.
[19] N.E. Gorji, H. Sohrabpoor, Modeling of light interference in $CH_3NH_3PbI_3Cl_x$ and $MAPbI_3Cl$ perovskite solar cells, Mater. Lett. 177 (2016) 143–147.
[20] E.D. Palik, Handbook of Optical Constants of Solids, Academic press, 1998.
[21] J. Kischkat, S. Peters, B. Gruska, M. Semtsiv, M. Chashnikova, M. Klinkmüller, O. Fedosenko, S. Machulik, A. Aleksandrova, G. Monastyrskyi, Mid-infrared optical properties of thin films of aluminum oxide, titanium dioxide, silicon dioxide, aluminum nitride, and silicon nitride, Appl. Opt. 51 (2012) 6789–6798.
[22] J.R. DeVore, Refractive indices of rutile and sphalerite, JOSA 41 (1951) 416–419.
[23] W. Li, Y. Shi, K. Chen, L. Zhu, S. Fan, A comprehensive photonic approach for solar cell cooling, ACS Photonics 4 (2017) 774–782.
[24] A.V. Tikhonravov, M.K. Trubetskov, G.W. DeBell, Application of the needle optimization technique to the design of optical coatings, Appl. Opt. 35 (1996) 5493–5508.
[25] V. Liu, S. Fan, S 4: a free electromagnetic solver for layered periodic structures, Comput. Phys. Commun. 183 (2012) 2233–2244.
[26] T.L. Bergman, A.S. Lavine, F.P. Incropera, D.P. Dewitt, Fundamentals of Heat and Mass Transfer, seventh ed., John Wiley & Sons, 2011.
[27] L. Zhu, A. Raman, K.X. Wang, M.A. Anoma, S. Fan, Radiative cooling of solar cells, Optica 1 (2014) 32–38.
[28] B. Lee, J. Liu, B. Sun, C. Shen, G. Dai, Thermally conductive and electrically insulating EVA composite encapsulants for solar photovoltaic (PV) cell, Express Polym. Lett. 2 (2008) 357–363.
[29] Y. Assoa, C. Menezo, G. Fraisse, R. Yezou, J. Brau, Study of a new concept of photovoltaic–thermal hybrid collector, Sol. Energy 81 (2007) 1132–1143.
[30] P. Gang, H. Fu, Z. Tao, J. Jie, A numerical and experimental study on a heat pipe PV/T system, Sol. Energy 85 (2011) 911–921.
[31] C. Guo, J. Ji, W. Sun, J. Ma, W. He, Y. Wang, Numerical simulation and experimental validation of tri-functional photovoltaic/thermal solar collector, Energy 87 (2015) 470–480.
[32] A.K. Das, M. Iqbal, A simplified technique to compute spectral atmospheric radiation, Sol. Energy 39 (1987) 143–155.
[33] S. Vall, A. Castell, Radiative cooling as low-grade energy source: a literature review, Renew. Sustain. Energy Rev. 77 (2017) 803–820.
[34] A. Berk, G.P. Anderson, P.K. Acharya, L.S. Bernstein, L. Muratov, J. Lee, M. Fox, S.M. Adler-Golden, J.H. Chetwynd, M.L. Hoke, MODTRAN5: 2006 update, Proc. SPIE (2006) 62331F.
[35] M. Hu, G. Pei, Q. Wang, J. Li, Y. Wang, J. Ji, Field test and preliminary analysis of a combined diurnal solar heating and nocturnal radiative cooling system, Appl. Energy 179 (2016) 899–908.
[36] D. Michell, K. Biggs, Radiation cooling of buildings at night, Appl. Energy 5 (1979) 263–275.
[37] Weather data. 〈http://energyplus.net/weather〉 (Accessed 21 March 2017).
[38] Chinese National Standard, GB 12021.3-2010, The Minimum Allowable Value of the Energy Efficiency and Energy Efficiency Grades for Room Air Conditioners, General Administration of Quality Supervision, Inspection and Quarantine of the PRC & Standardization Administration of the PRC, Beijing, 2010.
[39] L. Zhu, A. Raman, S. Fan, Color-preserving daytime radiative cooling, Appl. Phys. Lett. 103 (2013) 223902.